atmosphere

MDPI

Article

An Improved S-Band Polarimetric Radar-Based QPE Algorithm for Typhoons over South China Using 2DVD Observations

Zeyong Guo [1,2,3], Sheng Hu [4,*], Guangyu Zeng [2], Xingdeng Chen [2], Honghao Zhang [2], Feng Xia [4], Jiahui Zhuang [2], Min Chen [2] and Yuwen Fan [5]

1 Key Laboratory of Atmosphere Sounding, China Meteorological Administration, Chengdu 610225, China; guozeyong1982@163.com
2 Yangjiang Meteorological Bureau, China Meteorological Administration, Yangjiang 529500, China; zengguangyu@163.com (G.Z.); cgxgdg1985@163.com (X.C.); zhanghonghao0508@163.com (H.Z.); 18316100701@163.com (J.Z.); 18344090151@163.com (M.C.)
3 State Key Laboratory of Severe Weather, Chinese Academy of Meteorological Sciences, Beijing 100081, China
4 CMA/China Meteorological Administration Tornado Key Laboratory, Guangzhou Institute of Tropical and Marine Meteorology, Guangzhou 510641, China; xiaf@gd121.cn
5 Department of Atmospheric Sciences, College of Ocean and Meteorology, Huguang Campus, Guangdong Ocean University, Zhanjiang 524000, China; fanyuwen0126@163.com
* Correspondence: sheng_hu@gd121.cn

Abstract: Polarimetric radar data are an important tool for quantitative precipitation estimation (QPE), which is essential for monitoring and forecasting precipitation. Previous studies have shown that the drop size distribution (DSD) and polarimetric radar parameters of typhoon-induced precipitation differ significantly from those of other types of rainfall. South China is a region that frequently experiences typhoons and heavy rainfall, which can cause serious disasters. Therefore, it is critical to develop a QPE algorithm that is suitable for typhoon precipitation over South China. In this study, we constructed four simple QPE estimators, $R(Z_H)$, $R(Z_H, Z_{DR})$, $R(K_{DP})$ and $R(K_{DP}, Z_{DR})$ based on two-dimensional video disdrometer (2DVD) DSD observations of typhoon-induced precipitation over South China in 2017–2018. We analyzed the DSD characteristics and the estimation accuracy of these four QPE estimators in the reflectivity–differential reflectivity (Z_H–Z_{DR}) space, as well as the S-band polarimetric radar (S-POL) data of seven typhoon-induced precipitation events that affected South China in 2017–2019. We used these data to quantitatively determine the optimal ranges of the estimators and establish a typhoon precipitation QPE algorithm for typhoon-induced precipitation over South China (2DVD-Typhoon). The evaluation results showed that: (1) compared to $R(Z_H)$ and $R(K_{DP})$, $R(Z_H, Z_{DR})$ and $R(K_{DP}, Z_{DR})$ had lower performance in estimating typhoon-induced rainfall after incorporating the polarimetric parameter Z_{DR}, as strong crosswind of the typhoon caused some bias in the raindrop-induced ZDR; (2) the 2DVD-Typhoon algorithm utilizes the respective advantages of the individual estimators to generate the best QPE results; (3) the QPE performance of 2DVD-Typhoon and the Colorado State University–Hydrometeor Identification Rainfall Optimization (CSU-HIDRO) is used as a comparison for hourly rainfall, cumulative rainfall and different rainfall intensity. The comparison shows that 2DVD-Typhoon gives a better normalized error (NE), root mean square error (RMSE) and correlation coefficient (CC), indicating its strength in rainfall estimation for typhoons over South China. The above results provide theoretical support for improving typhoon-induced rainfall monitoring and numerical weather forecasting models in South China.

Keywords: quantitative precipitation estimation; drop size distribution; typhoon rainfall in South China; S-band polarimetric radar; two-dimensional video disdrometer

Citation: Guo, Z.; Hu, S.; Zeng, G.; Chen, X.; Zhang, H.; Xia, F.; Zhuang, J.; Chen, M.; Fan, Y. An Improved S-Band Polarimetric Radar-Based QPE Algorithm for Typhoons over South China Using 2DVD Observations. *Atmosphere* **2023**, *14*, 935. https://doi.org/10.3390/atmos14060935

Academic Editor: Tomeu Rigo

Received: 14 April 2023
Revised: 20 May 2023
Accepted: 22 May 2023
Published: 26 May 2023

1. Introduction

South China is the area most prone to typhoon disasters in China. On average, about 7.4 typhoons make landfall in South China each year, representing 60% of all typhoons

making landfall in China annually [1,2]. According to statistics, China suffers an annual economic loss of tens of billions of yuan as a direct result of typhoon disasters [3,4], posing a serious threat to people's lives and property. The intense precipitation brought on by typhoons after landfall is an important cause of typhoon disasters [5], making it crucial to monitor typhoon-induced precipitation with high accuracy. The polarimetric weather radar has unique advantages in precipitation monitoring. Quantitative precipitation estimation (QPE) by means of radar data inversion thus becomes an important method for monitoring typhoon-induced precipitation. Its accurate estimation accuracy provides a solid basis for the disaster prevention, mitigation and relief efforts of the government [6–8].

Rain rate, R, refers to the depth of surface water accumulated during a specific time period and is dependent on the equivalent volume diameter of raindrops. The radar reflectivity, Z_H is related to the drop size distribution (DSD). Based on this, a relationship between reflectivity and rain rate, Z_H–R, can be established. This is the physical basis of radar-based QPE [9]. For decades, scholars have studied QPE through the relationship between radar reflectivity, Z_H and rain rate, R, i.e., the Z_H–R relationship. Battan (1973) [10] compared 69 Z_H–R relationships and concluded that the estimation results of different Z_H–R relationships vary significantly. To quantify the QPE performance disparity across different precipitation types, scholars also have analyzed the Z_H–Z_{DR} distribution under these precipitation types using observed DSD data and found that significant variation exists in the performance of the Z_H–R relationship for different precipitation types [11,12]. To overcome the uncertainty of QPE inherited from the Z_H–R relationship, a rainfall estimation algorithm based on the polarimetric radar has been proposed. The first approach is the R(Z_H, Z_{DR}) algorithm first described by Seliga and Bringi (1976) [13], which uses the differential reflectivity, Z_{DR}, in combination with Z_H to reduce the impact of DSDs. The combined use of Z_H and Z_{DR} affords higher estimation accuracy than that of using Z_H alone [14,15]. However, a Z_{DR} bias of below 0.2 dB is needed to guarantee QPE accuracy and severe differential attenuation will lower the accuracy of R(Z_H, Z_{DR}), especially for C-band and X-band polarimetric radars [16,17]. Another approach is the use of the specific differential phase (K_{DP}) to establish the R(K_{DP}) algorithm. Compared to R(Z_H), R(K_{DP}) is less susceptible to the influence of DSDs [18,19]. In addition, hail and ground clutter have a relatively small impact on it [20–22]. The QPE algorithm R(K_{DP}, Z_{DR}), which uses a combination of K_{DP} and Z_{DR}, also offers a new direction [23,24]. This method shows improvement compared to using R(K_{DP}) [25–27] but is still subject to the effect of Z_{DR} calibration accuracy [28]. The above QPE algorithms have their unique advantages and disadvantages under different rainfall intensities and radar wavelengths. Combining multiple algorithms to establish a composite algorithm is also a helpful approach [29–31]. The most commonly used methods in the past have included the use of R(K_{DP}) or R(K_{DP}, Z_{DR}) for high rainfall intensities, R(Z_H, Z_{DR}) or R(Z_H) for low rainfall intensities and combining Z_H with the thresholds of Z_{DR} and K_{DP} or using the hydrometeor identification (HID) results as the basis for QPE algorithm selection [32–34]. For example, Wang et al. [35] established an optimized HCA-LIQ algorithm based on HID and the CSU-ICE algorithm [36]. The new algorithm showed improved estimation accuracy for light rain, heavy rain and rainstorms. Zhang et al. [37] performed a simulation and identified the piecewise fitting method (PFM) as the optimal QPE method for the polarimetric radar. They highlighted the importance of constructing localized QPE algorithms. In 2021, based on a constraint model obtained using raindrop size inversion [38], Guo et al. [39] established a QPE scheme (2DVD-SCM) for the South China monsoon using two-dimensional video disdrometers (2DVDs) and polarimetric radars located in South China. This algorithm achieves significantly higher estimation accuracy than the classic CSU-HIDRO algorithm in most monsoon-induced rainfall events, improving the QPE accuracy for South China monsoon-induced precipitation.

These scholars make full use of the unique advantages of the polarimetric weather radar in QPE to improve the accuracy of precipitation estimation by varying degrees.

However, significant differences exist in the QPE algorithms for different regions and precipitation systems [40]. Typhoon-induced precipitation systems in South China carry abundant water vapor and are subject to high wind speeds. Affected by strong crosswinds and a significant decrease in the terminal velocity of rain droplets, large rain droplets break apart easily, resulting in a small raindrop size, high particle number concentration and large raindrop deformation in typhoon-induced precipitation [41]. As such, there are significant differences between the DSD and microphysical characteristics of typhoon-induced precipitation in South China and other precipitation systems. These differences impose different requirements on the QPE algorithm for typhoon-induced precipitation compared to other precipitation systems. Thus, it is necessary to establish a separate QPE algorithm for typhoon-induced precipitation in South China.

To construct an optimized composite QPE algorithm for typhoon-induced precipitation in South China, the method of establishing a QPE algorithm based on the normalized errors (NEs) of Z_H–Z_{DR} distribution is adopted from Chen et al. [42], which mainly focuses on the monsoon-affected summer precipitation in East China and used three QPE estimators, $R(Z_H)$, $R(Z_H, Z_{DR})$ and $R(K_{DP})$, based on the C-band polarimetric radar, to construct a composite algorithm. Differently, in this paper, we use 2DVD-generated DSD data of typhoons in South China to obtain four QPE estimators, $R(Z_H)$, $R(Z_H, Z_{DR})$, $R(K_{DP})$ and $R(K_{DP}, Z_{DR})$ by fitting the polarimetric parameters of the S-band polarimetric radar, and the performance differences of these four QPE estimators are reflected in the distribution of their estimation accuracy in the reflectivity–differential reflectivity (Z_H–Z_{DR}) space and integrating their respective optimal intervals. The performance of this algorithm is evaluated quantitatively in detail.

2. Observation Data and Pre-Processing

Seven large-scale precipitation events triggered by typhoons that made landfall in South China in the period 2017–2019 were selected for inclusion in the study. Of the seven events, Typhoon Ewiniar (1804) had a continued impact of 4 days, bringing with it the highest average accumulated rainfall (156.6 mm) and highest hourly rainfall (120.8 mm) as recorded on the rain gauge. Typhoon Mangkhut (1822), on the other hand, featured the highest accumulated rainfall (1844 mm).

Figure 1 shows the trajectory and intensity change of the seven typhoons selected for this study. Figure 2 shows the location map of the two radars, 2DVDs and surface rain gauge stations in Guangzhou and Yangjiang. The 2DVD drop size distribution data used in this study were recorded in 2017–2018, while the radar and rain gauge data were recorded in 2017–2019. Table 1 lists the basic information about these rainfall events. The number of hourly rainfall samples in the table indicates the number of hourly rainfall events observed by the rain gauges after quality control during typhoon precipitation.

Table 1. Data for typhoon-induced precipitation events.

Typhoon Name (Identification Code)	Observation Period (World Time)	Number of Rain Gauges	Maximum Hourly Rainfall (mm/h)	Maximum Accumulated Rainfall (mm)	Average Accumulated Rainfall (mm)	Number of Volume Scans	Sample Size of Hourly Rainfall
Merbok (1702)	12–13 June 2017	110	46.5	70.8	12.8	2200	220
Hato (1713)	22 August 2017	152	33.5	41.2	11.9	3700	370
Mawar (1716)	3–4 September 2017	625	71.9	198.7	27.6	21,570	2157
Ewiniar (1804)	4–8 June 2018	1039	120.8	897.8	156.6	158,400	15,840
Mangkhut (1822)	16–17 September 2018	989	70.2	1844	96.7	107,210	10,721
Mun (1904)	3–4 July 2019	965	46.4	269.6	14.4	33,910	3391
Wipha (1907)	31 July–1 August 2019	1043	68.5	863.1	56.4	85,960	8596

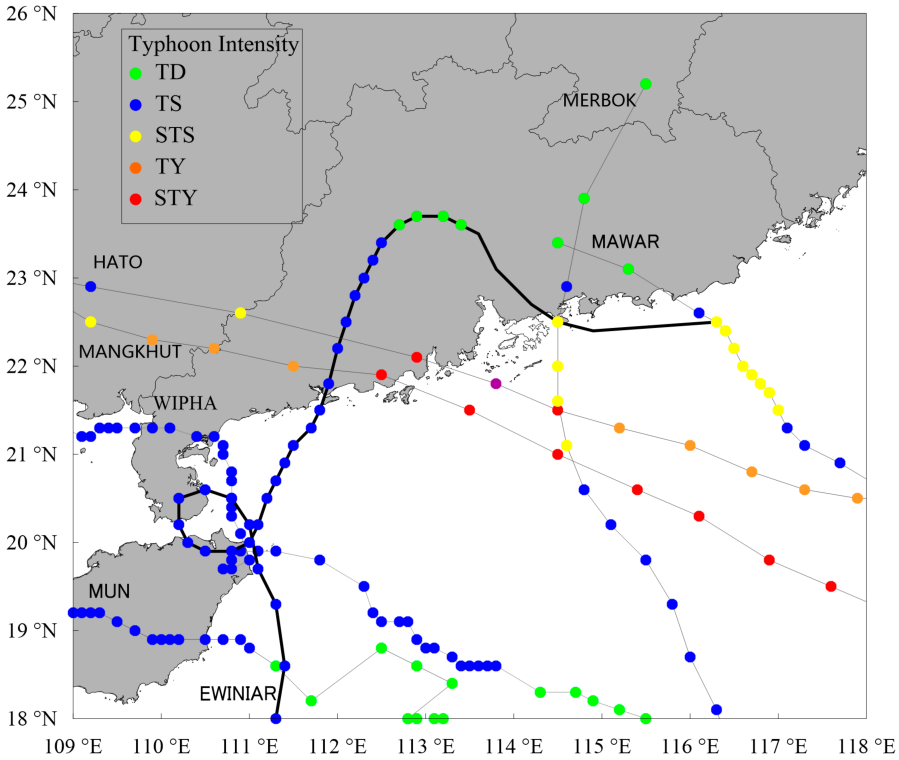

Figure 1. Trajectory and intensity change of typhoons (TD: tropical depression, TS: tropical storm, STS: severe tropical storm, TY: typhoon, STY: severe typhoon).

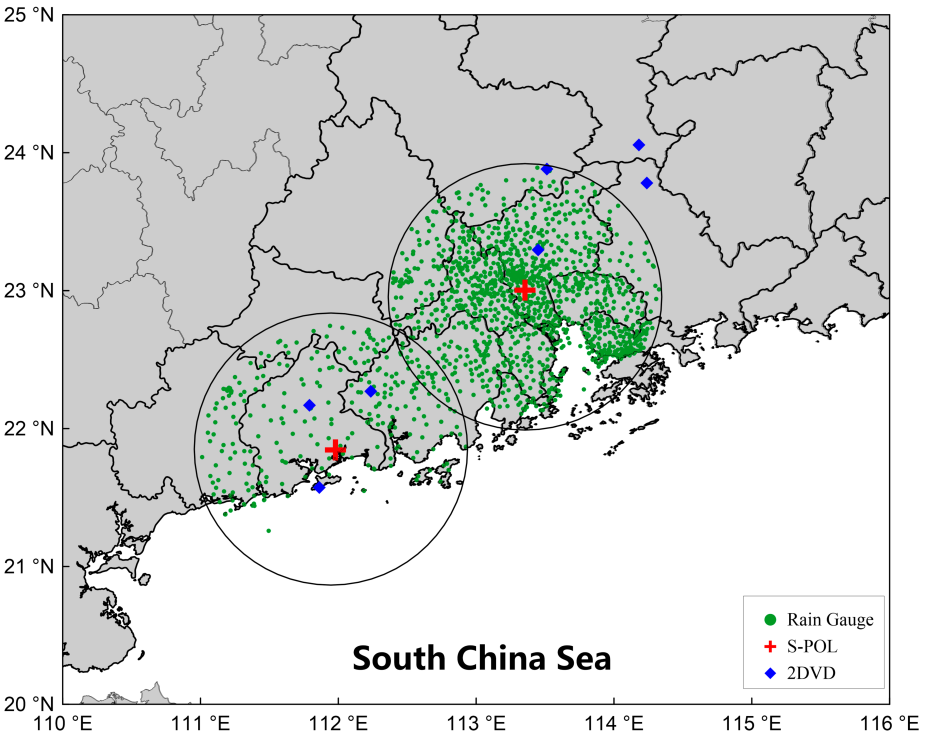

Figure 2. The location map of the two radars, 2DVDs and surface rain gauge stations in Guangzhou and Yangjiang. (Red crosses represent the locations of the two S-band polarimetric radars (S-POL) in Guangzhou and Yangjiang, Guangdong Province; green dots indicate the locations of the rain gauges within the area covered by the radars (5–100 km radius); blue diamonds represent the 2DVDs of the Longmen Cloud Physics Field Experiment Base of the China Meteorological Administration (CMA)).

2.1. Rain Gauge Rainfall Data and Pre-Processing

The rainfall data from the 1043 rain gauge stations within the radar observation range of Guangzhou and Yangjiang were used to evaluate the study. These rain gauges feature a rainfall resolution of 0.1 mm. Rainfall data observation and transmission were made every 5 min, including 1-min rainfall and 5-min accumulated rainfall. The radars take 6 min to complete a set of volume scans. Thus, the 1-min rainfall data from the rain gauges were added up to generate the 6-min rainfall, so as to align the timing of estimated rainfall from the radar with that of the observed rainfall from the rain gauges. In this study, the observed rainfall data at these stations were used as the evaluation criteria for QPE.

To minimize the interference of observation anomaly from rain gauges with the performance evaluation of the QPE algorithm, inverse distance weighting (IDW) was used here to select automated rain gauges in terms of spatial consistency [43–45]. As shown in Figure 3, Rain gauges giving reliable data were used to perform correction on the polarimetric radar-based QPE algorithm in order to obtain more accurate initial precipitation of radar QPE. For rain gauges with suspected faults that were inconsistent with the value calculated using the IDW method, the initial precipitation of radar QPE was used to perform a second-time validation of the estimated rainfall data, thus reducing erroneous judgments arising from the use of spatial consistency alone as the selection criterion.

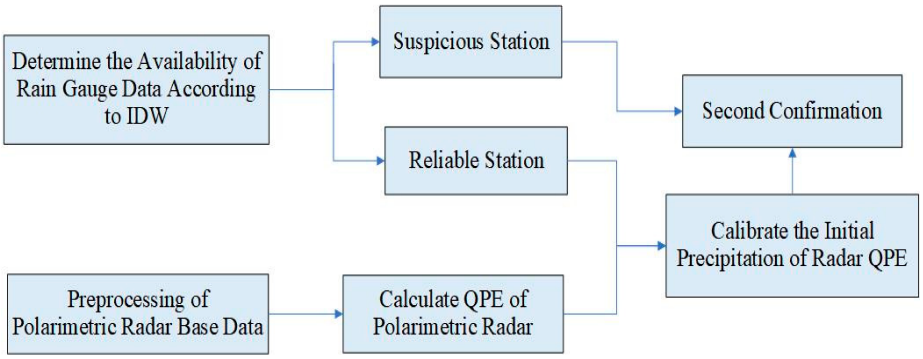

Figure 3. Quality control process of rain gauge data.

2.2. Drop Size Distribution Data and Pre-Processing

The DSD data used in this study were obtained from the 2DVD of the Longmen Cloud Physics Field Experiment Base, China Meteorological Administration (CMA) [46]. The station distribution is as shown in Figure 2.

Errors were found to be present in the data recorded by the 2DVD [47]. To improve the quality of the observed DSD data, based on previous results, the following observed values were eliminated as noise: those in which the total number of particles in the diameter channel and velocity channel was less than 50, the rainfall intensity was less than 0.5 mm/h or the absolute value of the difference between the final falling velocity of raindrops and the theoretical final velocity was greater than 0.6 times the theoretical final velocity [48,49]. The theoretical final velocity of precipitation particles was calculated using the suggested method by Feng (2020) [41] and Wu (2020) [50].

A total of 79,122 typhoon-induced rainfall DSD samples were made available for analysis in this study. The sample size refers to the number of observations made by disdrometers (1-min average) during the typhoon-induced precipitation process.

2.3. Polarimetric Radar Data and Pre-Processing

A polarimetric radar provides additional polarimetric parameters such as Z_{DR}, K_{DP}, correlation coefficient (CC) and Φ_{DP}. These observed values are smaller in magnitude than Z_H and are more prone to observation errors. QPE accuracy is closely related to the quality of radar data, thus putting higher demand on the data quality of Z_{DR} and K_{DP}. The calibration error of Z_{DR} needs to be within 0.2 dB in general and within 0.1 dB for

estimating light rain [16]. The K_{DP} of rainfall echo also needs to be non-negative. For these reasons, to solve the data quality issue of polarimetric radars, elimination of non-rainfall echo, correction of the Z_{DR} bias of the radar system and suppression of the random jitter in the differential phase (Φ_{DP}) were performed in this study for data quality control [51–54].

Both S-band polarimetric radars in Guangzhou and Yangjiang (as GZ S-POL and YJ S-POL) were operated with a volume coverage pattern (VCP21). To reduce interference from the melting layer and ground clutter, observation data recorded at an elevation angle of 1.5° and 5–100 km of the radar station (i.e., the circular area bounded by the two circles in Figure 2) were used. A total of 412,950 base data points were collected from the seven typhoon events included in the study. The number of radar volume scans performed for each typhoon event is shown in Table 1.

2.4. QPE Algorithm Evaluation

To evaluate the effectiveness of the QPE algorithm, the estimated hourly rainfall and observed hourly rainfall data were compared. The normalized error (NE), root mean square error (RMSE) and CC between the two were calculated [39], as follow Equations (1)–(3). NE represents the deviation between the estimated value and the measured value; the smaller the value, the higher the accuracy and credibility of precipitation estimation. RMSE reflects the degree to which radar-estimated rainfall deviates from the measured value of a rain gauge; the smaller the value, the more concentrated the distribution of deviations and the better the algorithm stability. CC is a dimensionless quantity between 0–1, which represents the degree of closeness of the correlation between the estimated values and measured values; the closer it is to 1, the higher the correlation. These three values were used as the metrics to evaluate the QPE algorithm in this study.

$$NE = \frac{\sum_{i=1}^{N} \left| R_{radar} - R_{gauge} \right|}{\sum_{i=1}^{N} R_{gauge}} \quad (1)$$

$$RMSE = \sqrt{\frac{1}{N} \sum_{i=1}^{N} \left(\left| R_{radar} - R_{gauge} \right| - ME \right)^2} \quad (2)$$

$$CC = \frac{\sum_{i=1}^{N} \left(R_i^{gauge} - \overline{R_i^{gauge}} \right) \left(R_i^{radar} - \overline{R_i^{radar}} \right)}{\sqrt{\sum_{i=1}^{N} \left(R_i^{gauge} - \overline{R_i^{gauge}} \right)^2 \sum_{i=1}^{N} \left(R_i^{radar} - \overline{R_i^{radar}} \right)^2}} \quad (3)$$

3. Establishing The 2DVD-Typhoon Algorithm

The technical procedure for establishing the South China Typhoon QPE algorithm (2DVD-Typhoon) is shown in Figure 4. Four simple QPE estimators, $R(Z_H)$, $R(Z_H, Z_{DR})$, $R(K_{DP})$ and $R(K_{DP}, Z_{DR})$, were constructed using inversion of observed surface drop size distribution. The optimal interval for the estimation performance of these four QPE estimators in the Z_H–Z_{DR} space was then quantitatively calculated and the optimal combination was found to establish a composite QPE algorithm, 2DVD-Typhoon. In the last step, the estimation performance of the 2DVD-Typhoon algorithm was evaluated using a dense array of surface rain gauges.

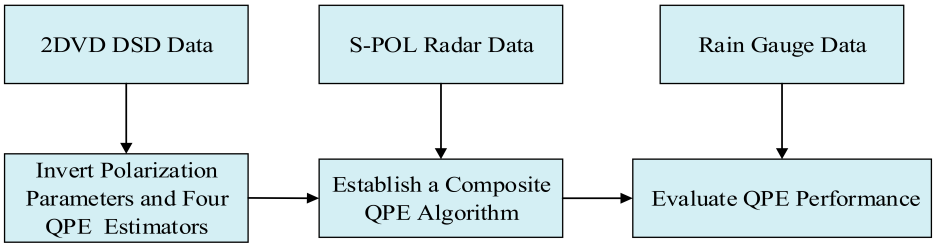

Figure 4. Technical procedures for establishing the South China typhoon QPE scheme (2DVD-Typhoon).

3.1. Establishing Simple QPE Estimators Using 2DVD Drop Size Distributions

The DSD data on typhoon-induced precipitation systems were collected from seven 2DVDs during 2017–2018. Following the method of Wang et al. [51] in constructing an S-band polarimetric radar simulator, four simple typhoon QPE estimators, $R(Z_H)$, $R(Z_H, Z_{DR})$, $R(K_{DP})$ and $R(K_{DP}, Z_{DR})$, were constructed. The specific QPE estimators are as follows:

$$R(Z_H) = 0.0212{Z_H}^{0.72}, \quad (4)$$

$$R(Z_H,Z_{DR}) = 0.00366{Z_H}^{0.880}{Z_{DR}}^{-0.745}, \quad (5)$$

$$R(K_{DP}) = 56.805{K_{DP}}^{0.87}, \quad (6)$$

$$R(K_{DP}, Z_{DR}) = 51.523{Z_{DR}}^{-0.692}{K_{DP}}^{0.972}. \quad (7)$$

The units of polarimetric radar parameters for Equations (4)–(7) were: dBZ for Z_H, dB for Z_{DR} and degree per kilometer for K_{DP}.

To analyze the performance of the four QPE estimators (Equations (4)–(7)), the retrieved rainfall data were compared to the rainfall data observed by 2DVD. The results are shown in the scatterplots of Figure 5. It was found that $R(K_{DP}, Z_{DR})$ has the lowest RMSE and NE, the highest CC and the best performance, followed by $R(K_{DP})$ and $R(Z_H, Z_{DR})$, with the latter two both being superior to $R(Z_H)$.

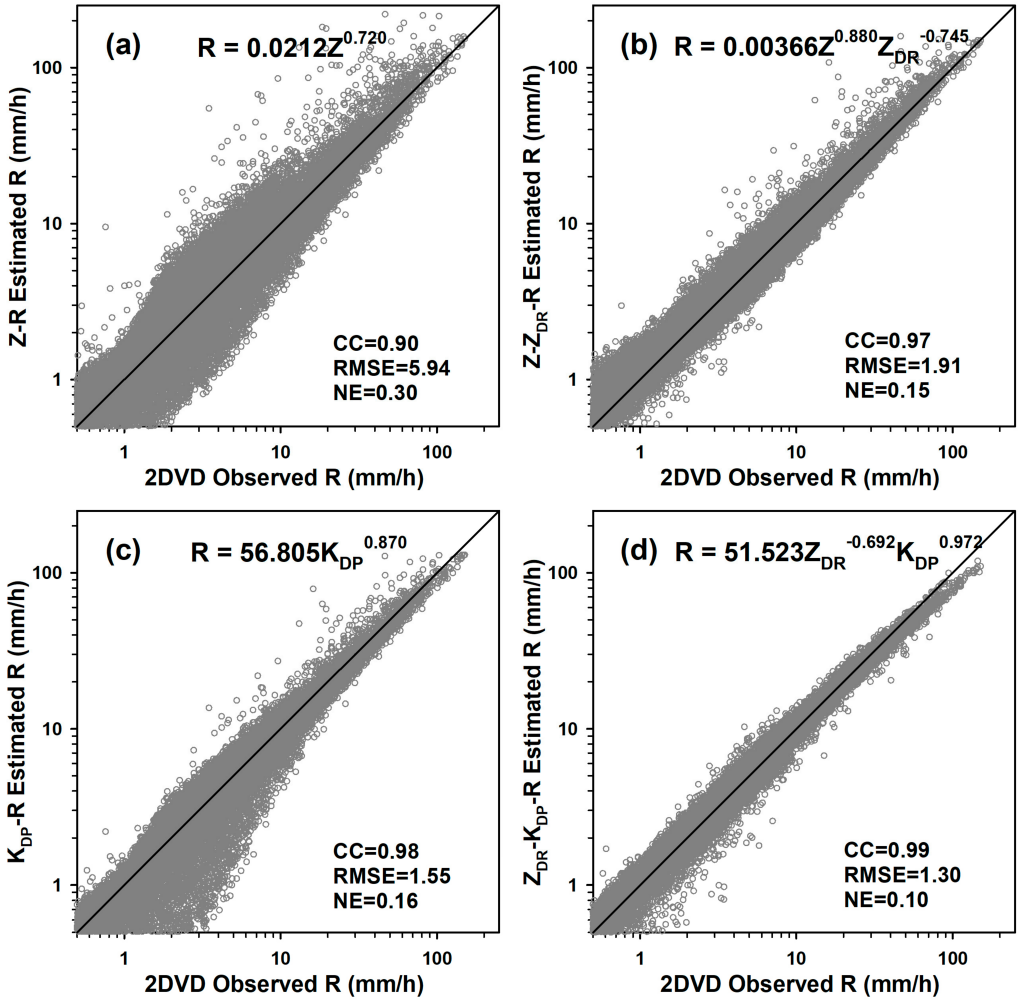

Figure 5. Scatterplot of rain rate retrieved from (**a**) $R(Z_H)$, (**b**) $R(Z_H, Z_{DR})$, (**c**) $R(K_{DP})$ and (**d**) $R(K_{DP}, Z_{DR})$ vs. the directly observed rain rate from the 2DVDs during typhoon precipitation from 2017 to 2018.

3.2. Establishing the Composite QPE Algorithm Using the Quantitative Distribution Interval of the Performance of Simple QPE Estimators in Z_H–Z_{DR} Space

3.2.1. Error Distribution Characteristics of Simple QPE Estimators

Using the radar observation data in Table 1 and Equations (4)–(7), the estimated hourly rainfall was calculated using a radar. Comparing this to the observed hourly rainfall by surface rain gauges, the distribution of average NE for the four simple QPE estimators in the Z_H–Z_{DR} space was obtained, as shown in Figure 6. Figure 6a shows the distribution of all hourly rainfall samples for all typhoon events listed in Table 1. Figure 6b–e show the NE distribution for the four simple QPE estimators in the Z_H–Z_{DR} space. The average spatial scale of these plots is 0.25 km, the temporal scale is 1 h and the Z_H axis and Z_{DR} axis have an interval of 2 dBZ and 0.2 dB, respectively. The colored squares represent the average values of NE.

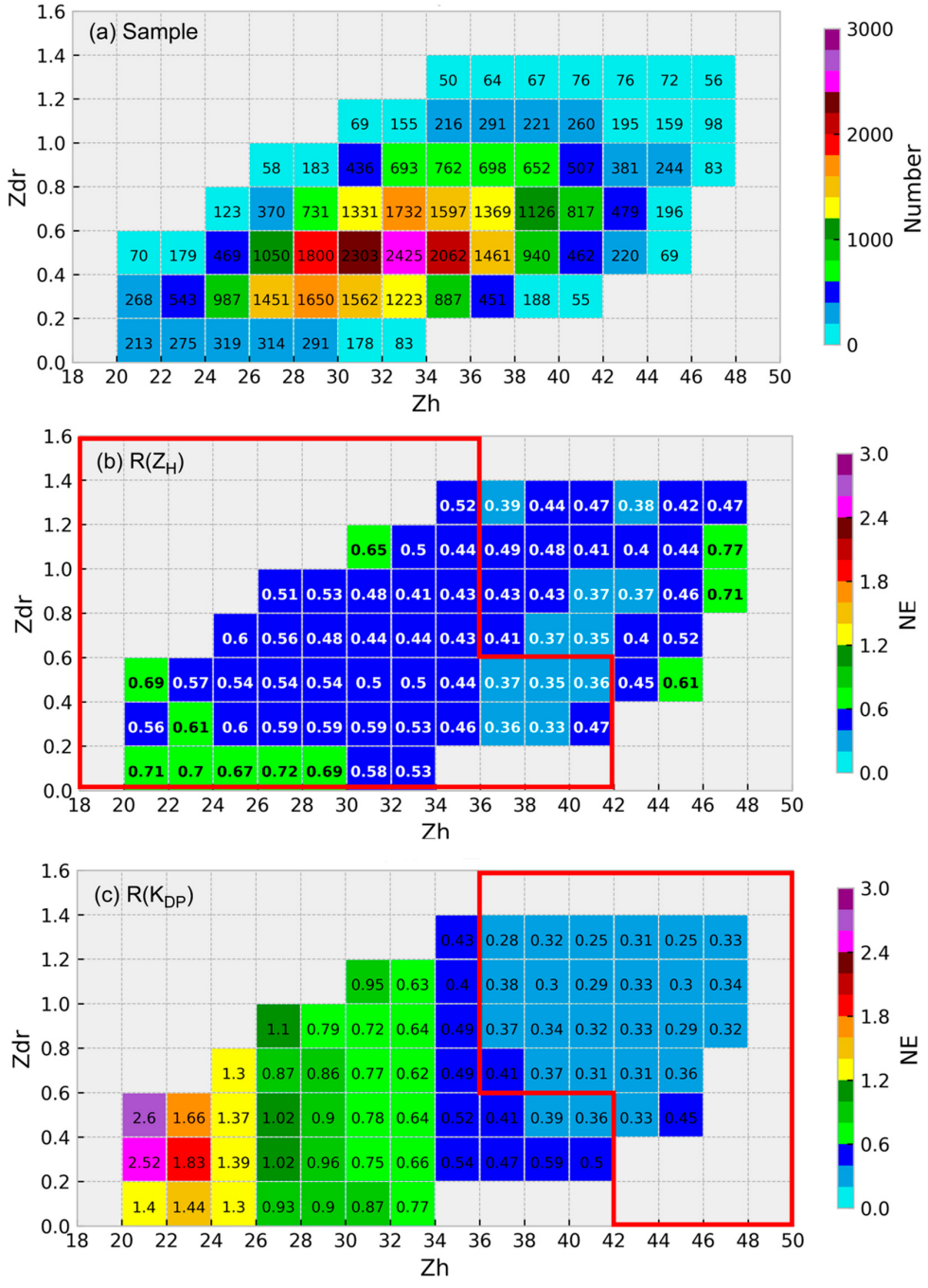

Figure 6. *Cont.*

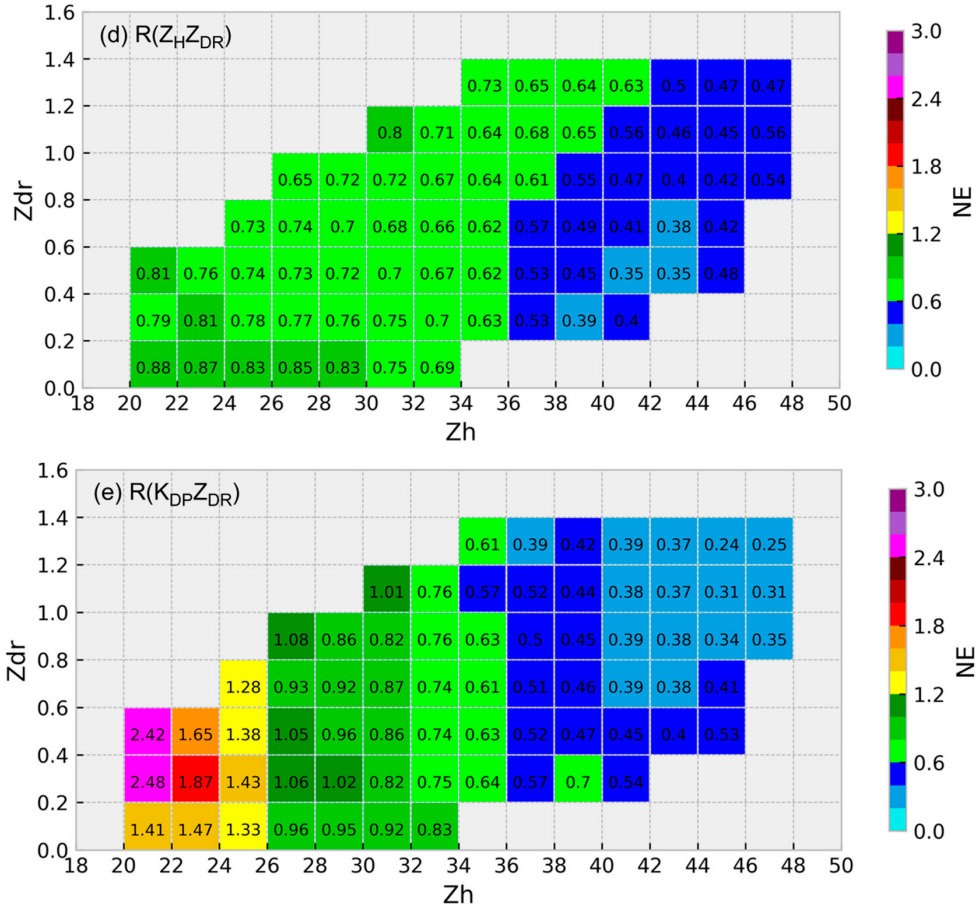

Figure 6. The total sample number (**a**), hourly QPE normalized error of (**b**) R(Z_H), (**c**) R(Z_H, Z_{DR}), (**d**) R(K_{DP}) and (**e**) R(K_{DP}, Z_{DR}) for all seven typhoon precipitation events in Z_H–Z_{DR} space; red lines in (**b**,**c**) represent the optimal threshold ranges of the four single QPE estimators used to calculate the composite QPE algorithm (2DVD-Typhoon).

It should be noted that in order to make the results more generalizable, data with sample sizes below 50 were excluded from this study. Thus, only five typhoon-induced precipitation events, namely Mawar (1716), Ewiniar (1804), Mangkhut (1822), Mun (1904) and Wipha (1907), were evaluated.

As shown in Figure 6a, the Z_H of a large number of samples is concentrated in the 22–42 dBZ interval, while the Z_{DR} is concentrated in the 0.2–1.0 dB interval, reflecting the microphysical characteristics in which small-sized raindrops of typhoons play a more prominent role. Comparing the NE distribution of the four simple QPE estimators in the Z_H–Z_{DR} space (Figure 6b–e), it can be seen that they all exhibit distinct intervals, i.e., $Z_H < 36$ dBZ, 36 dBZ $\leq Z_H \leq$ 42 dBZ and $Z_H > 42$ dBZ in terms of Z_H distribution. In the interval $Z_H < 36$ dBZ, the NE values of R(Z_H) mostly fall below 0.6, with some exceptions. This indicates a better performance of R(Z_H) compared to the other three QPE estimators. In the interval 36 dBZ $\leq Z_H \leq$ 42 dBZ, at $Z_{DR} < 0.6$ dB, although the NE values of the other three QPE estimators are all below 0.6, R(Z_H) still performs better; at $Z_{DR} \geq 0.6$ dB, R(K_{DP}) becomes stronger; at $Z_H > 42$ dBZ, R(K_{DP}) undoubtedly shows the best performance, with R(K_{DP}, Z_{DR}) trailing slightly behind. Both estimators are nevertheless far superior to R(Z_H). R(Z_H, Z_{DR}) has no advantage over the other three QPE estimators in any interval.

In theory, adding a polarimetric parameter, Z_{DR}, that characterizes particle size should more accurately describe the DSD characteristics of a typhoon. However, the inclusion of Z_{DR} in this paper deteriorates the QPE performance. For a more intuitive characterization of the impact of the typhoon on Z_{DR}, the estimated rainfall by R(K_{DP}, Z_{DR}) and R(Z_H, Z_{DR}) was compared to the observed rainfall using a rain gauge. As can be seen from Figure 7a–d,

compared to R(Z_H) and R(K_{DP}), after incorporating Z_{DR}, R(Z_H, Z_{DR}) and R(K_{DP}, Z_{DR}) significantly underestimated the rainfall to a greater degree. This underestimation was more pronounced for R(Z_H) and R(Z_H, Z_{DR}) in areas with higher average instantaneous wind speeds (AIWS). For example, in areas with AIWS greater than 14 m/s, the ratio of QPE/Gauge for R(Z_H, Z_{DR}) was generally lower than 0.3, while the ratio for R(Z_H) was typically between 0.3 and 0.6. It is thus safe to conclude that for typhoon-induced precipitation, the deterioration of QPE performance after Z_{DR} inclusion is directly related to the higher-than-usual Z_{DR} bias of raindrops caused by strong crosswinds.

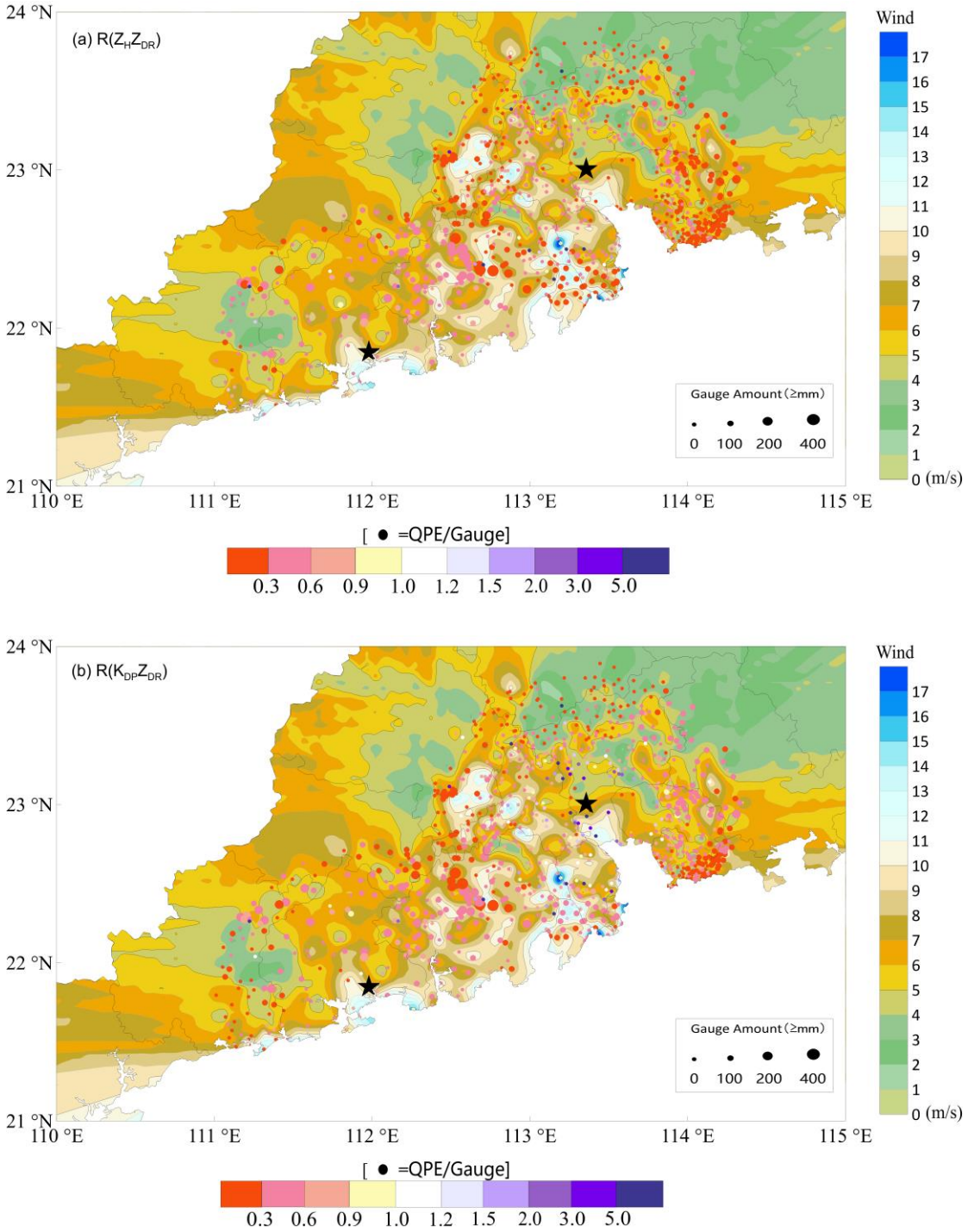

Figure 7. *Cont.*

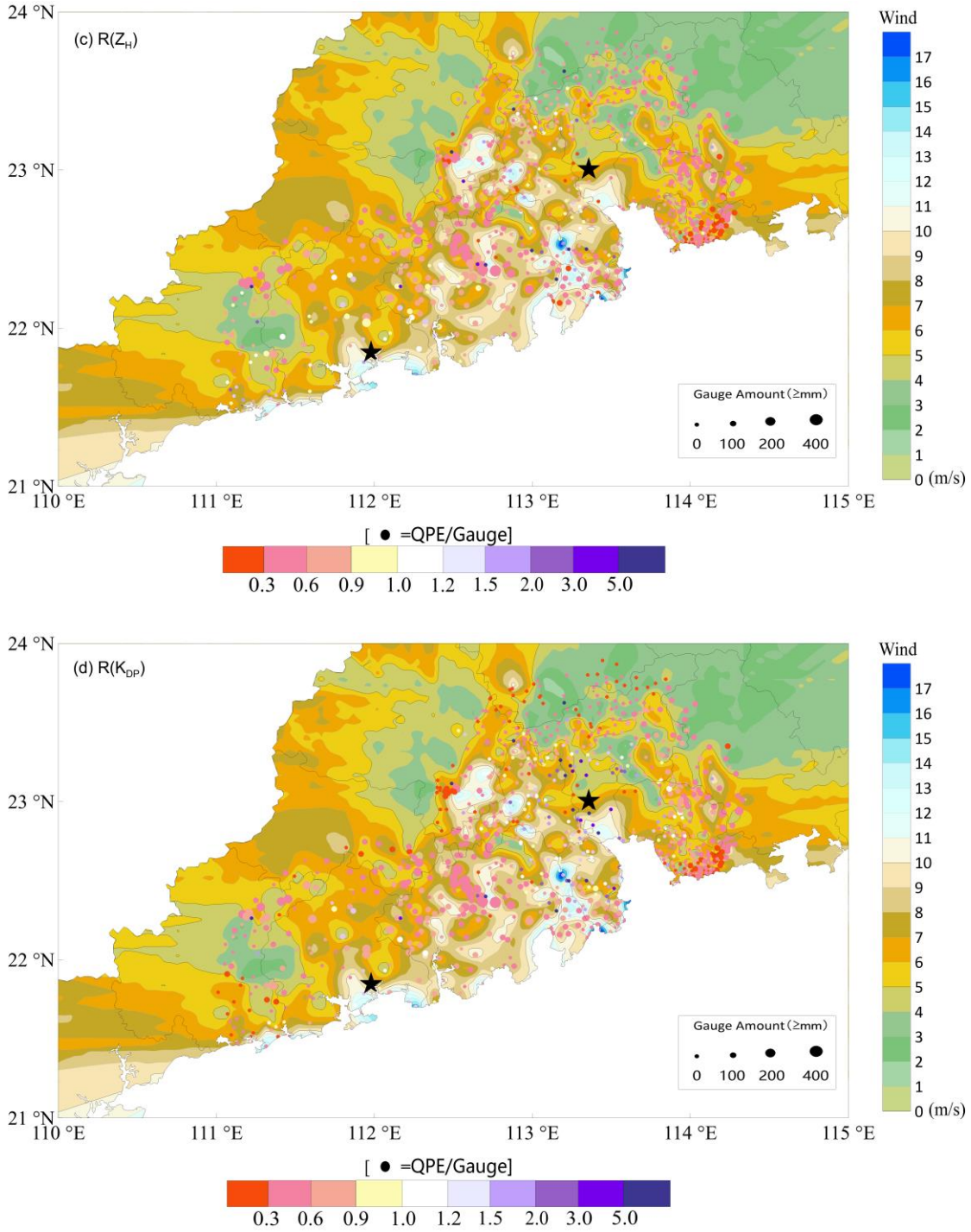

Figure 7. The ratio diagrams of estimated cumulative precipitation derived from (**a**) R(Z_H, Z_{DR}), (**b**) R(K_{DP}, Z_{DR}), (**c**) R(Z_H) and (**d**) R(K_{DP}) to rain gauge cumulative precipitation (The stars in the figure are the locations of the two S-band polarimetric radars (S-POL) in Guangzhou and Yangjiang, Guangdong Province. The scatter points in the figure are the locations of the rain gauge stations. The size of the scatter point represents the cumulative rainfall of the station and the color of the scatter point represents the ratio of QPE to the rain gauge. The filled contours represent the average instantaneous wind speed).

3.2.2. Establishing a Composite QPE Algorithm (2DVD-Typhoon)

Based on the previous analysis, a composite QPE algorithm, 2DVD-Typhoon, was proposed using the NE distribution characteristics of the four simple QPE estimators in the

Z_H–Z_{DR} space. The Z_H interval and Z_{DR} interval corresponding to the minimum NE were selected to construct this composite QPE algorithm:

$R(K_{DP})$ is used when $Z_H \geq 36$ dBZ and $Z_{DR} \geq 0.6$ dB or $Z_H \geq 42$ dB. $R(K_{DP})$ cannot be used when $K_{DP} < 0.1$. It is, thus, necessary to add $K_{DP} \geq 0.1^\circ$/km as an additional constraint. In all other cases, $R(Z_H)$ is used.

In 2DVD-Typhoon, the coefficients for $R(Z_H)$ and $R(K_{DP})$ are obtained by fitting DSD data and are only used when Z_H, Z_{DR} and K_{DP} reach their respective thresholds. In the following sections, a detailed evaluation will be conducted on the radar-based estimated values obtained with 2DVD-Typhoon and the observed values obtained with the rain gauge.

4. Evaluation of the 2DVD-Typhoon Algorithm

4.1. Comparison of the Composite QPE Algorithm with the Simple QPE Estimators in the Cumulative Rainfall of Each Typhoon Rainfall Event

Table 2 provides a comparison of the evaluation results of 2DVD-Typhoon and the simple QPE estimators in the hourly rainfall of each typhoon rainfall event; the column "Total rainfall" represents the sum of all five subsequent typhoons. All three evaluation criteria for typhoon processes indicate better performance of $R(Z_H)$ and $R(K_{DP})$ compared to $R(Z_H, Z_{DR})$ and $R(K_{DP}, Z_{DR})$, respectively. With reference to the results of Section 3.2, this more explicitly shows that the incorporation of Z_{DR} lowers the estimation performance of $R(Z_H, Z_{DR})$ and $R(K_{DP}, Z_{DR})$. For both a single typhoon-induced rainfall event and all typhoon-induced rainfall events, 2DVD-Typhoon shows the lowest NE and RMSE and the highest CC, indicating that, compared to the four simple QPE estimators, the estimated rainfall of 2DVD-Typhoon is more consistent with the observed rainfall and that the proposed composite QPE algorithm is robust.

Table 2. Performance comparison of 2DVD-Typhoon algorithm with simple QPE estimators.

Parameter	Equation	Typhoon Process					
		Total Rainfall	**Mawar (1716)**	**Ewiniar (1804)**	**Mangkhut (1822)**	**Mun (1904)**	**Wipha (1907)**
NE (fraction)	2DVD-Typhoon	0.41	0.36	0.35	0.49	0.53	0.43
	$R(Z_H)$	0.45	0.38	0.40	0.50	0.65	0.47
	$R(Z_H, Z_{DR})$	0.58	0.52	0.59	0.66	0.49	0.45
	$R(K_{DP})$	0.51	0.46	0.43	0.58	0.73	0.59
	$R(K_{DP}, Z_{DR})$	0.60	0.53	0.53	0.66	0.73	0.67
RMSE (mm)	2DVD-Typhoon	5.791	4.78	5.953	6.838	4.038	4.862
	$R(Z_H)$	6.308	4.975	6.811	7.005	4.728	5.152
	$R(Z_H, Z_{DR})$	7.814	6.306	9.197	8.684	3.625	5.19
	$R(K_{DP})$	7.084	5.388	7.627	7.68	5.456	6.304
	$R(K_{DP}, Z_{DR})$	7.931	6.054	8.718	8.559	5.387	6.984
CC	2DVD-Typhoon	0.808	0.882	0.865	0.714	0.746	0.754
	$R(Z_H)$	0.765	0.871	0.854	0.708	0.852	0.779
	$R(Z_H, Z_{DR})$	0.719	0.856	0.825	0.669	0.84	0.753
	$R(K_{DP})$	0.743	0.869	0.793	0.654	0.577	0.636
	$R(K_{DP}, Z_{DR})$	0.675	0.861	0.728	0.585	0.492	0.553

4.2. Comparison of 2DVD-Typhoon with the Classic CSU-HIDRO QPE Algorithm

4.2.1. Comparison Using all Samples

The CSU-HIDRO algorithm was developed by Colorado State University and it has been improved over time by incorporating dual-polarization radar data. This algorithm utilizes a combination of four rain-rate estimators similar to this article, while a hydrometeor identification (HID) algorithm was required to be able to filter out solid precipitation. In some cases, it has shown better performance than other QPE algorithms [36]. Figure 8a–d compares the performance of 2DVD-Typhoon with the classic CSU-HIDRO algorithm. From

the evaluation criteria shown in Figure 8a,c, 2DVD-Typhoon achieves better results on NE (40.98), RMSE (5.791 mm) and CC (0.808). From the accumulated rainfall in Figure 8b,d, the scatter points of 2DVD-Typhoon are more concentrated, while those of CSU-HIDRO are more diffused and show a more significant underestimation.

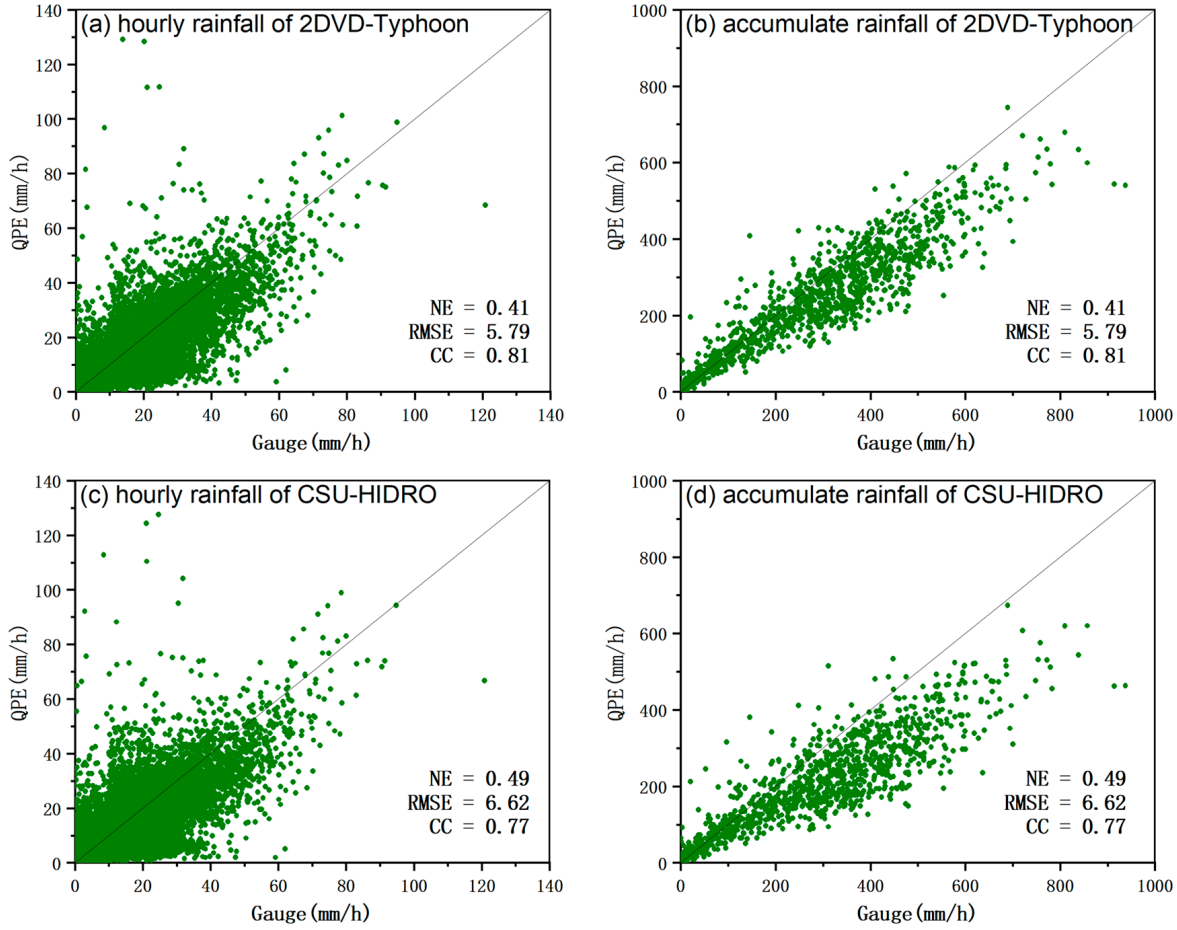

Figure 8. Scattered plots comparing the two algorithms: hourly rainfall (**a**) and accumulated rainfall (**b**) of 2DVD-Typhoon, hourly rainfall (**c**) and accumulated rainfall (**d**) of CSU-HIDRO.

4.2.2. Comparison by Rain Intensity

To further evaluate the performance of the two types of algorithms under different rain intensities, the rain intensities of all typhoon events listed in Table 2 were grouped into three intervals: 0–10 mm/h, 10–20 mm/h and above 20 mm/h. Values of the evaluation criteria for 2DVD-Typhoon and CSU-HIDRO were calculated under different rain intensities. Figure 9 shows the evaluation results for the two QPE algorithms.

For hourly rainfall of 0–10 mm/h or 10–20 mm/h, 2DVD-Typhoon returns significantly better NE than CSU-HIDRO. For $10 \leq R < 20$, the NE difference between the two is 11.42%. In terms of RMSE and CC, 2DVD-Typhoon is also superior to CSU-HIDRO. For hourly rainfall of above 20 mm, 2DVD-Typhoon returns slightly better NE than CSU-HIDRO. Hence, as indicated by the values of NE, RMSE and CC, 2DVD-Typhoon delivers a better estimation performance under various rain intensities.

The above results indicate that 2DVD-Typhoon is a more robust algorithm in estimating typhoon-induced precipitation systems than the CSU-HIDRO algorithm, whether the comparison is made using all samples or based on rain intensity classification.

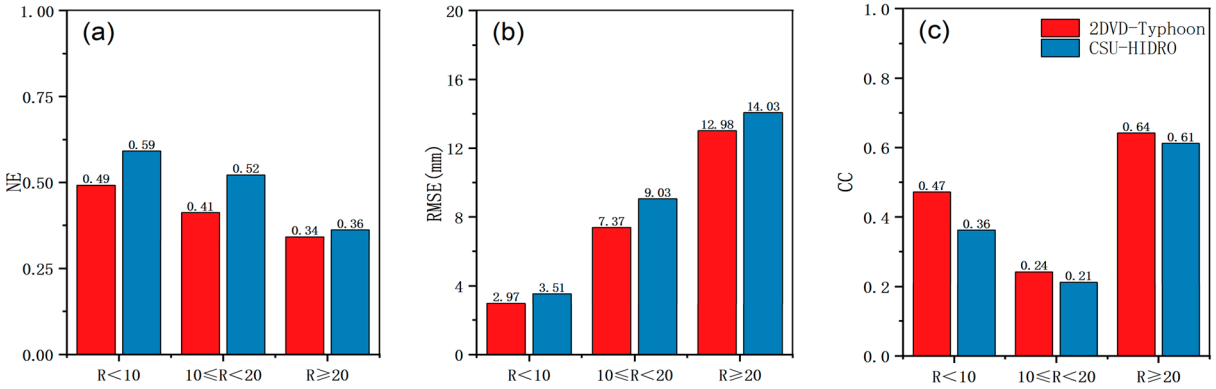

Figure 9. Evaluation of the two algorithms under different rainfall intensities.(Comparison of, (**a**) NE, (**b**) RMSE, (**c**) cc, between 2DVD-Typhoon and CSU-HIDRO).

5. Discussion and Conclusions

This study utilizes surface drop size distribution data, polarimetric radar data and surface rain gauge data to construct an algorithm (2DVD-Typhoon) applicable to typhoon-induced rainfall estimation in South China and evaluates its performance. The main research findings are as follows:

(1) A comparison of R(Z_H), R(Z_H, Z_{DR}), R(K_{DP}) and R(K_{DP}, Z_{DR}) reveals a better estimation performance of R(Z_H) and R(K_{DP}) than R(Z_H, Z_{DR}) and R(K_{DP}, Z_{DR}), largely due to the negative impact of the polarimetric parameter Z_{DR}. Quantitative investigation shows that, due to the influence of strong crosswinds brought on by the typhoon, the excessively large Z_{DR} bias of raindrops leads to significant underestimation by R(Z_H, Z_{DR}) and R(K_{DP}, Z_{DR}).

(2) For each typhoon-induced rainfall event, 2DVD-Typhoon returns better values for the evaluation criteria compared to the simple QPE estimators. This is mainly because the 2DVD-Typhoon algorithm is able to quantitatively obtain the optimal intervals of the four simple QPE estimators, thereby fully utilizing the advantages of each simple QPE estimator and producing the best QPE results.

(3) Compared to the classic CSU-HIDRO algorithm, 2DVD-Typhoon performs better on hourly rainfall, accumulated rainfall and across rainfall intensities, as indicated by the NE, RMSE and CC values. In the comparison using all samples, 2DVD-Typhoon yields better NE (40.98), RMSE (5.791 mm) and CC (0.808). In the comparison by rain intensity classification, 2DVD-Typhoon shows a higher estimation performance in all three rain intensity intervals: $0 < R < 10$, $10 \leq R < 20$ and $R \geq 20$. The NE of 2DVD-Typhoon is 11.42% lower than that of CSU-HIDRO in the rainfall interval of $10 \leq R < 20$.

In this study, it was found that R(K_{DP}, Z_{DR}) still outperforms R(K_{DP}) on a small portion of samples at large Z_H and Z_{DR}, likely because these samples are less affected by typhoon crosswinds, such that raindrops have not produced significant Z_{DR} bias. A slight improvement in the values of the evaluation criteria is therefore observed after the inclusion of Z_{DR}. However, to make the results of this study more generic, data with sample sizes below 50 were eliminated. In the future, with the addition of these raindrop samples that are less affected by typhoon crosswinds, it is possible for R(K_{DP}, Z_{DR}) to outperform R(K_{DP}) in some intervals. Quantitatively specifying the optimal interval of the R(K_{DP}, Z_{DR}) will further improve the performance of the South China Typhoon QPE algorithm.

Author Contributions: Conceptualization, S.H.; Investigation, Z.G., G.Z., X.C., H.Z. and F.X.; Supervision, S.H.; Data analysis, Z.G., G.Z., X.C., H.Z., J.Z., M.C. and Y.F.; Writing—original draft preparation, Z.G., G.Z., X.C. and H.Z.; Writing—review and editing, S.H. and F.X. All authors have read and agreed to the published version of the manuscript.

Funding: This research was supported by the Opening Foundation of Key Laboratory of Atmosphere Sounding, the China Meteorological Administration and the CMA Research Centre on Meteorological Observation Engineering Technology (U2021Z04); the Open Grants of the state Key Laboratory of Severe Weather (2020LASW-B04); Guangdong Science and Technology Special Fund Project (SDZX202208); National Natural Science Foundation of China (U22422203, 42030610, 41975138, 41975046, 42075086, 42275008).

Institutional Review Board Statement: Not applicable.

Informed Consent Statement: Not applicable.

Data Availability Statement: The data presented in this study are available from China Meteorological Data Service Center at the website of http://data.cma.cn (accessed on 10 April 2023).

Conflicts of Interest: The authors declare no conflict of interest.

References

1. Ying, M.; Zhang, W.; Yu, H.; Lu, X.; Feng, J.; Fan, Y.; Zhu, Y.; Chen, D. An Overview of the China Meteorological Administration Tropical Cyclone Database. *J. Atmos. Ocean. Technol.* **2014**, *31*, 287–301. [CrossRef]
2. Xu, G.; Xian, D.; Fournier-Viger, P.; Li, X.; Ye, Y.; Hu, X. AM-ConvGRU: A spatio-temporal model for typhoon path prediction. *Neural Comput. Appl.* **2022**, *34*, 5905–5921. [CrossRef]
3. Chen, W.; Lu, Y.; Sun, S.; Duan, Y.; Leckebusch, G.C. Hazard Footprint-Based Normalization of Economic Losses from Tropical Cyclones in China During 1983–2015. *Int. J. Disaster Risk Sci.* **2018**, *9*, 195–206. [CrossRef]
4. Gao, Y.; Wang, H.; Liu, G.M.; Sun, X.Y.; Fei, X.Y.; Wang, P.T.; Lv, T.T.; Xue, Z.S.; He, Y.W. Risk assessment of tropical storm surges for coastal regions of China. *J. Geophys. Res. Atmos.* **2014**, *119*, 5364–5374. [CrossRef]
5. Zhao, H.; Duan, X.; Raga, G.B.; Klotzbach, P.J. Changes in Characteristics of Rapidly Intensifying Western North Pacific Tropical Cyclones Related to Climate Regime Shifts. *J. Clim.* **2018**, *31*, 8163–8179. [CrossRef]
6. Zhang, P.C.; Du, B.Y.; Dai, T.P. *Radar Meteorology*; China Meteorological Press: Beijing, China, 2001. (In Chinese)
7. Hu, M.B.; Gao, T.C.; Tang, D.Z. *Analysis and Application of Doppler Radar Data*; People's Liberation Army Press: Beijing, China, 2000. (In Chinese)
8. Liu, L.P.; Ge, R.S.; Zhang, P.Y. A Study of Method and Accuracy of Rainfall Rate and Liquid Water Content Measurements by Dual Linear Polarization Doppler Radar. *Chin. J. Atmos. Sci.* **2002**, *26*, 709–719. (In Chinese) [CrossRef]
9. Marshall, J.S.; Palmer, W. The distribution of raindrops with size. *J. Meteorol.* **1948**, *5*, 165–166. [CrossRef]
10. Battan, L.J. *Radar Observations of the Atmosphere*; The University of Chicago Press: Chicago, IL, USA, 1973; p. 324.
11. Schuur, T.J.; Ryzhkov, A.V.; Clabo, D.R. Climatological analysis of DSDs in Oklahoma as revealed by 2D-video disdrometer and polarimetric WSR-88D. In Proceedings of the 32nd Conference on Radar Meteorology in Alvarado GH CD-ROM, Albuquerque, NM, USA, 22–28 October 2015.
12. Ryzhkov, A.; Diederich, M.; Zhang, P.; Simmer, C. Potential Utilization of Specific Attenuation for Rainfall Estimation, Mitigation of Partial Beam Blockage, and Radar Networking. *J. Atmos. Ocean. Technol.* **2014**, *31*, 599–619. [CrossRef]
13. Seliga, T.A.; Bringi, V.N. Potential Use of Radar Differential Reflectivity Measurements at Orthogonal Polarizations for Measuring Precipitation. *J. Appl. Meteorol. Climatol.* **1976**, *15*, 69–76. [CrossRef]
14. Liu, L.; Qian, Y.; Wang, Z.; Chu, R. Comparitive Study on Dual Linear Polarization Radar Measuring Rainfall Rate. *Chin. J. Atmos. Sci.* **1996**, *20*, 615–619. (In Chinese) [CrossRef]
15. Chen, H.; Chandrasekar, V.; Bechini, R. An Improved Dual-Polarization Radar Rainfall Algorithm (DROPS2.0): Application in NASA IFloodS Field Campaign. *J. Hydrometeorol.* **2017**, *18*, 917–937. [CrossRef]
16. Ryzhkov, A.V.; Giangrande, S.E.; Schuur, T.J. Rainfall estimation with a polarimetric prototype of the WSR-88D radar. *J. Appl. Meteorol.* **2005**, *44*, 502–515. [CrossRef]
17. Zrnić, D.; Doviak, R.; Zhang, G.; Ryzhkov, A. Bias in Differential Reflectivity due to Cross Coupling through the Radiation Patterns of Polarimetric Weather Radars. *J. Atmos. Ocean. Technol.* **2010**, *27*, 1624–1637. [CrossRef]
18. Sachidananda, M.; Zrnic, D.S. Differential propagation phase shift and rainfall rate estimation. *Radio Sci.* **1986**, *21*, 235–247. [CrossRef]
19. Sachidananda, M.; Zrnić, D.S. Rain Rate Estimates from Differential Polarization Measurements. *J. Atmos. Ocean. Technol.* **1987**, *4*, 588–598. [CrossRef]
20. Balakrishnan, N.; Zrnić, D.S. Estimation of Rain and Hail Rates in Mixed-Phase Precipitation. *J. Atmos. Sci.* **1990**, *47*, 565–583. [CrossRef]

21. Ryzhkov, A.V.; Zrnic, D.S. Polarimetric Rainfall Estimation in the Presence of Anomalous Propagation. *J. Atmos. Ocean. Technol.* **1998**, *15*, 1320–1330. [CrossRef]
22. Ryzhkov, A.; Kumjian, M.; Ganson, S.; Zhang, P. Polarimetric radar characteristics of melting hail. Pt II: Practical implications. *J. Appl. Meteorol. Climatol.* **2013**, *52*, 2871–2886. [CrossRef]
23. Jameson, A.R. A Comparison of Microwave Techniques for Measuring Rainfall. *J. Appl. Meteorol.* **1991**, *30*, 32–54. [CrossRef]
24. Ryzhkov, A.V.; Zrnić, D.S. Comparison of Dual-Polarization Radar Estimators of Rain. *J. Atmos. Ocean. Technol.* **1995**, *12*, 249–256. [CrossRef]
25. Petersen, W.A.; Carey, L.D.; Rutledge, S.A.; Knievel, J.C.; Johnson, R.H.; Doesken, N.J.; McKee, T.B.; Haar, T.V.; Weaver, J.F. Mesoscale and Radar Observations of the Fort Collins Flash Flood of 28 July 1997. *Bull. Am. Meteorol. Soc.* **1999**, *80*, 191–216. [CrossRef]
26. Ryzhkov, A.; Zhang, P.; Krause, J.; Schuur, T.; Palmer, R.; Zrnic, D. Simultaneous measurements of precipitation using S-band and C-band polarimetric radars. *J. Iahs Aish Publication.* **2012**, *351*, 87–92.
27. Thompson, E.J.; Rutledge, S.A.; Dolan, B.; Thurai, M.; Chandrasekar, V. Dual-Polarization Radar Rainfall Estimation over Tropical Oceans. *J. Appl. Meteorol. Clim.* **2018**, *57*, 755–775. [CrossRef]
28. Maki, M.; Park, S.-G.; Bringi, V. Effect of Natural Variations in Rain Drop Size Distributions on Rain Rate Estimators of 3 cm Wavelength Polarimetric Radar. *J. Meteorol. Soc. Jpn. Ser. II* **2005**, *83*, 871–893. [CrossRef]
29. Chandrasekar, V.; Gorgucci, E.; Scarchilli, G. Optimization of Multiparameter Radar Estimates of Rainfall. *J. Appl. Meteorol.* **1993**, *32*, 1288–1293. [CrossRef]
30. Matrosov, S.; Kingsmill, D.; Ralph, F. The utility of X-band polarimetric radar for quantitative estimates of rainfall parameters. *J. Hydrometeorol.* **2005**, *6*, 248–262. [CrossRef]
31. Giangrande, S.E.; Krause, J.M.; Ryzhkov, A.V. Automatic Designation of the Melting Layer with a Polarimetric Prototype of the WSR-88D Radar. *J. Appl. Meteorol. Clim.* **2008**, *47*, 1354–1364. [CrossRef]
32. Figueras i Ventura, J.; Tabary, P. The new French operational polarimetric radar rainfall rate product. *J. Appl. Meteorol. Climatol.* **2013**, *52*, 1817–1835. [CrossRef]
33. Cifelli, R.; Chandrasekar, V.; Lim, S.; Kennedy, P.C.; Wang, Y.; Rutledge, S.A. A New Dual-Polarization Radar Rainfall Algorithm: Application in Colorado Precipitation Events. *J. Atmos. Ocean. Technol.* **2011**, *28*, 352–364. [CrossRef]
34. Yu, Z.; Xian-Tong, L.; Bing-Hong, C.; Jia-Bao, F.; Lin, Z.; Cong-Cong, T. Application of X-band Polarimetric Phased-array Radars in Quantitative Precipitation Estimation. *J. Trop. Meteorol.* **2023**, *29*, 142–152. [CrossRef]
35. Wang, D.; Liu, L.P.; Wu, C. An Optimization Rainfall Algorithm of S Band Dual Polarization Radar Based on Hydrometeor Identification. *J. Meteorol. Mon.* **2017**, *43*, 1041–1051. (In Chinese)
36. Cifelli, R.; Barjenbruch, D.; Brunkow, D.; Carey, L.; Davey, C.; Doesken, N.; Gimmestad, C.; Huse, T.; Kennedy, P.; Rutledge, S.A. Evaluation of an operational polarimetric rainfall algorithm. In Proceedings of the 31st International Conference on Radar Meteorology, Seattle, WA, USA, 7 August 2003.
37. Yang, Z.; Li-ping, L.; Hao, W.; Chao, C.; Han, W.; Bao-zhu, X. Development and assessment of quantitative precipitation estimation algorithms for S-, C-, and X-band dual-polarization radars based on disdrometer data from three regions of China. *J. Trop. Meteorol.* **2019**, *25*, 269–292.
38. Liu, X.; Wan, Q.; Wang, H.; Xiao, H.; Zhang, Y.; Zheng, T.; Feng, L. Raindrop Size Distribu-tion Parameters Retrieved from Guangzhou S-band Polarimetric Radar Observations. *J. Meteorol. Res.* **2018**, *32*, 571–583. [CrossRef]
39. Guo, Z.; Hu, S.; Liu, X.; Chen, X.; Zhang, H.; Qi, T.; Zeng, G. Improving S-Band Polarimetric Radar Monsoon Rainfall Estimation with Two-Dimensional Video Disdrometer Observations in South China. *Atmosphere* **2021**, *12*, 831. [CrossRef]
40. Lu, F.; Sheng, H.; Xian-Tong, L.; Hui-Qi, L.; Hui, X.; Xiao-Hui, L.; Rui-Ze, L.; Qing, L. Comparison of Microphysical Characteristics Between Warm-sector and Frontal Heavy Rainfall in the South of China. *J. Trop. Meteorol.* **2023**, *29*, 87–100. [CrossRef]
41. Feng, L.; Hu, S.; Liu, X.; Xiao, H.; Pan, X.; Xia, F.; Ou, G.; Zhang, C. Precipitation Microphysical Characteristics of Typhoon Mangkhut in Southern China Using 2D Video Disdrometers. *Atmosphere* **2020**, *11*, 975. [CrossRef]
42. Chen, G.; Zhao, K.; Zhang, G.; Huang, H.; Liu, S.; Wen, L.; Yang, Z.; Yang, Z.; Xu, L.; Zhu, W. Improving Polarimetric C-Band Radar Rainfall Estimation with Two-Dimensional Video Disdrometer Observations in Eastern China. *J. Hydrometeorol.* **2017**, *18*, 1375–1391. [CrossRef]
43. Wang, H.Y.; Wang, G.L.; Liu, L.P.; Jiang, Y.; Wang, D.; Li, F. Development of a real-time quality control method for automatic rain gauge data using radar quantitative precipitation estimation. *Chin. J. Atmos. Sci.* **2015**, *39*, 59–67. (In Chinese)
44. Wu, H.Y.; Li, Z.H.; Li, W.Y.; Zheng, J. Characteristics Analysis of Extremly Severe Precipitation Based on Regional Automatic Weather Stations in Guangdong. *J. Meteorol. Mon.* **2020**, *46*, 801–812. (In Chinese)
45. Jing, G.F.; Luo, L.; Xiao, H.; Guo, J.; Cui, X. Application Research of Dual-Polarization Radar in Quality Control of Automatic Rain Gauge. *J. Meteorol. Mon.* **2020**, *46*, 1189–1198. (In Chinese)
46. Xian-Tong, L.; Zheng, R.; Sheng, H.; Qi-Lin, W.; Li-Ping, L.; Ya-Li, L.; Zhi-Qun, H.; Hui-Qi, L.; Hui, X.; Wei-Yan, L.; et al. The Longmen Cloud Physics Field Experiment Base, China Meteorological Administration. *J. Trop. Meteorol.* **2023**, *29*, 1–15. [CrossRef]
47. Tokay, A.; Petersen, W.A.; Gatlin, P.; Wingo, M. Comparison of raindrop size distribution measurements by collocated disdrometers. *J. Atmos. Ocean. Technol.* **2013**, *30*, 1672–1690. [CrossRef]
48. Jaffrain, J.; Berne, A. Experimental Quantification of the Sampling Uncertainty Associated with Measurements from PARSIVEL Disdrometers. *J. Hydrometeorol.* **2011**, *12*, 352–370. [CrossRef]

49. Liu, X.; Li, H.; Hu, S.; Wan, Q.; Xiao, H.; Zheng, T.; Li, M.; Ye, L.; Guo, Z.; Wang, Y.; et al. A High-precision and Fast Solution Method of Gamma Raindrop Size Distribution based on 0-Moment and 3-Moment in South China. *J. Appl. Meteorol. Clim.* **2021**, *60*, 1407–1421. [CrossRef]
50. Wu, C. *Data Quality Analysis, Hydrometeor Classification and Mosaic Application of Polarimetric Radar in China*; Nanjing University of Information Science and Technology: Nanjing, China, 2018. (In Chinese)
51. Wang, H.; Wan, Q.L.; Yin, J.F.; Ding, W.Y. Application of the dual-polarization radar data in numerical modeling studies: Construction of the simulator. *Acta Meteorol. Sin.* **2016**, *74*, 229–243.
52. Huang, H. *A Research on Optimization-Based Rainfall Parameter Retrieval Using Polarimetric Radar Data*; Nanjing University: Nanjing, China, 2018. (In Chinese)
53. Zhang, Y.; Liu, L.; Wen, H.; Wu, C.; Zhang, Y. Evaluation of the Polarimetric-Radar Quantitative Precipitation Estimates of an Extremely Heavy Rainfall Event and Nine Common Rainfall Events in Guangzhou. *Atmosphere* **2018**, *9*, 330. [CrossRef]
54. Guo, Z.; Hu, D.; Ma, J.; Li, Z.; Yao, Z.; Sun, Z. Quality Control Analysis and Effect Evaluation for S-band Dual Polarimetric Radar. In Proceedings of the ICFEICT 2021: International Conference on Frontiers of Electronics, Information and Computation Technologies, Changsha, China, 21–23 May 2021. (In Chinese).